IEEE Access
Multidisciplinary | Rapid Review | Open Access Journal

Received December 31, 2018, accepted January 22, 2019, date of publication January 25, 2019, date of current version February 12, 2019.

*Digital Object Identifier 10.1109/ACCESS.2019.2895415*

# An Optimal Low Complexity PAPR Reduction Technique for Next Generation OFDM Systems

**AHMAD M. RATEB[1], (Member, IEEE), AND MOHAMED LABANA[2], (Student Member, IEEE)**
[1]Faculty of Electronic and Information Engineering, Huaiyin Institute of Technology, Huai'an 223002, Jiangsu, China
[2]Department of Electrical and Computer Engineering, Gina Cody School of Engineering and Computer Science, Concordia University, Montreal, QC H3G 1M8, Canada

Corresponding author: Ahmad M. Rateb (ahmadmrateb@ieee.org)

**ABSTRACT** Orthogonal frequency division multiplexing (OFDM) is an efficient multi-carrier modulation technique that underlies most of the current and probably future high-speed wireless communication systems. However, the OFDM waveform is characterized by a high peak-to-average power ratio (PAPR), especially when a large number of subcarriers are used. A high PAPR is a major waveform defect since it leads to non-linear distortion when passing through the transmitter's power amplifier. Most of the PAPR reduction techniques found in the literature reduce the PAPR mainly at the cost of either excessive computational complexity or degrading the transmission bit error rate (BER). We propose a low-complexity technique for PAPR reduction based on linear scaling of a portion of signal coefficients by an optimal factor. This paper is backed up by the extensive analysis of various performance metrics, which leads to optimal choices of key parameters and hence maximum achievable gains. The analytic and simulated results show that the proposed technique is capable of reducing the PAPR effectively with negligible effect on BER in return for a slight reduction in data rate. For example, for 1024 subcarriers, the PAPR can be reduced from 13 dB to below 7.4 or 6.9 dB, in return for only 1% or 2% reduction in data rate, respectively. In addition, the achievable PAPR varies very slightly in response to increasing the number of subcarriers. This offers a highly competitive and flexible tradeoff compared with those provided by current techniques found in the literature. Therefore, this technique has a very good potential for practical application in current and future OFDM-based systems, especially those which employ a very large number of subcarriers, such as LTE, DVB-T2, and 5G systems.

**INDEX TERMS** Orthogonal frequency division multiplexing (OFDM), peak to average power ratio (PAPR), optimization, 5G, distortionless techniques, signal distortion techniques, companding, peak clipping, DVB-T2, LTE, low-complexity.

## I. INTRODUCTION

The demand for new and improved wireless multimedia services such as High Definition (HD) video streaming, tactile internet, virtual reality and multiplayer gaming is growing higher everyday. This demand creates a vital need for higher data rates, larger network capacity and lower latency. In addition, higher energy efficiency has become a priority since most user devices are currently battery operated [1]. The long awaited next generation 5G mobile network is expected to achieve 100x higher speed and capacity compared to the current 4G network, with network latency as low as 1 ms [2]–[4]. In addition, the network will support Machine-Type-Communication (MTC) required by millions of Internet-of-Things (IoT) devices that are expected to be connected to the network [5], [6].

Orthogonal Frequency Division Multiplexing (OFDM) is the current state-of-the art technique underlying most of today's wireless communication systems. To name a few, Long-Term Evolution (LTE) [7], Worldwide Interoperability for Microwave Access (WiMAX) [8], IEEE 802.11 a/g/n/ac/ax [9], [10] and Digital Video Broadcast (DVB-T1/2) [11], [12]. The major strengths of OFDM are high spectral efficiency, bandwidth flexibility, ability to combat multipath fading effects, and ability to coexist with other systems sharing the same band [13], [14]. In addition, OFDM

The associate editor coordinating the review of this manuscript and approving it for publication was Emrecan Demirors.

is highly compatible with Multiple-Input-Multiple-Output (MIMO) systems, which is expected to play a central role in 5G systems [15], [16].

OFDM and OFDM-based waveforms are expected to continue to exist in 5G mobile systems [2], [17]–[19]. For example, [20] proposed an OFDM-based scheme called Flexible Configured OFDM (FC-OFDM) that is designed to be optimum for multi-service environment, which is one of the distinguishable properties of 5G networks. It offers both very high-rate and very low-rate connectivity to devices within the network. In addition, filtered OFDM (f-OFDM) [19], [21], [22] waveform is a strong candidate for 5G applications, which relaxes stringent synchronization requirements in regular OFDM and maximizes spectrum utilization.

However, due to the fact that the OFDM signal is produced by subjecting data symbols (arranged in the form of a set of subcarriers) to an Inverse Fast Fourier Transform (IFFT), there is a high possibility that a subset of these symbols add up coherently, leading to the production of some large peaks at the output. This phenomenon is usually quantified in terms of Peak to Average Power Ratio (PAPR), which is proportional to the number of subcarriers [23], [24]. High PAPR signals are highly undesirable since large magnitude spikes cause non-linear distortion when passed through the power amplifier prior to transmission, which degrades system performance. On the other hand, backing off the operating point of the power amplifier to accommodate these spikes within the linear region severely reduces the efficiency of the amplifier, leading to low Signal-to-Noise Ratio (SNR) at the receiver [25], [26]. Nevertheless, employing a power amplifier with large dynamic range has a high cost.

The problem of high PAPR is even more significant in 5G systems, since 5G systems are planned to rely on utilizing mm-wave frequency ranges, to be able to satisfy the demand for large bandwidth [27]–[29]. It was shown that mm-wave power amplifiers perform poorly, and produce higher levels of distortion upon operating in the saturation region [1], [30], [31]. Therefore, PAPR minimization is highly crucial in 5G OFDM-based systems.

Numerous techniques have been proposed for PAPR reduction over the past decade [26], [32], [33]. These methods will be reviewed in more detail in the next section. In general, there are three main performance criteria which any PAPR reduction method makes a trade-off between them. These criteria are the level of signal distortion, spectral efficiency and computational complexity. Any PAPR reduction technique would favor one or two criteria at the cost of the other/s. The level of distortion caused by PAPR reduction is critical since it impacts the overall transmission Bit Error Rate (BER) of the system. On the other hand, some techniques rely on transmitting side information bits to the receiver. These bits carry information regarding the parameters used by the PAPR reduction technique, which will help the receiver restore the original OFDM waveform. Hence, transmitting these bits alongside the original data diminishes the overall spectrum efficiency of the system. Finally, techniques characterized by high computational complexity require more expensive computational hardware, and would consume more power, which is unfavorable for battery-operated mobile devices.

In this paper, we propose a very low-complexity technique that minimizes the PAPR of the OFDM waveform with minimum waveform distortion, at the expense of allocating an arbitrarily small portion of the available bandwidth for transmission of side information, which can be controlled by the system designer. We show analytically and numerically that the PAPR of the OFDM waveform can be reduced to an arbitrarily small value regardless or the number of sub-carriers or baseband modulation order. In order to optimize the trade-off between PAPR reduction and distortion, we introduce the notion of *net gain* of the proposed technique, where we assess it not only in terms of PAPR reduction, but also by incorporating the losses due to signal distortion that occurs upon transmitting the signal over a noisy channel. Therefore, a positive net gain implies actual overall improvement in system performance. This enables us to ensure the optimality of the selected parameters by which they provide maximum net gain, rather than only minimize PAPR. In addition, we perform a detailed analysis of the number and type of computations required by our technique, and derive an explicit expression of the number of computations. We show that this technique has a linear computational complexity at the transmitter and sub-linear complexity at the receiver, relying almost entirely on basic arithmetic operations such as addition, multiplications and divisions.

The remainder of this paper is arranged as follows: in Section II, we review the related literature on PAPR reduction techniques. We introduce our proposed technique in section III, and then analyze its performance section IV in terms of PAPR, distortion and spectral efficiency. In Section V, we describe our approach for selection of optimal values for different parameters relevant to the proposed technique, which lead to the best achievable performance. In Section VI, we describe the overall operation of the proposed technique in the form of executable algorithms, and analyze their computational complexity in detail. In Section VII, we present simulated results comparing the proposed technique to various techniques from related literature, and discuss these results. Finally, we draw our conclusions in section VIII.

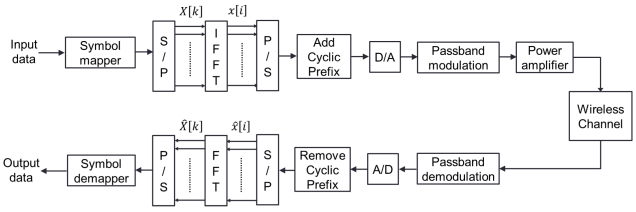


**FIGURE 1.** Block diagram of OFDM transmitter and receiver.

## II. PAPR REDUCTION TECHNIQUES

Consider an OFDM system constructed with MQAM symbol mapping, and $N$ subcarriers, as shown in Fig. 1. The samples of the baseband time-domain signal $x[i]$, $i = 0, 1, \ldots, N-1$ generated at the output of the IFFT block are expressed as

$$x[i] \triangleq \frac{1}{\sqrt{N}} \sum_{k=0}^{N-1} X[k] \exp\left(j\frac{2\pi}{N}ki\right) \tag{1}$$

where $X[k]$, $k = 0, 1, \ldots, N-1$ is the vector of MQAM-mapped data symbols. By definition, the PAPR of the baseband signal $x[i]$ is given by [24], [32]:

$$\rho_x := \frac{\max_i\{|x[i]|^2\}}{p_x} \tag{2}$$

where $\max\{|x[i]|^2\}$ is the is the maximum instantaneous subcarrier power across the OFDM symbol, and $p_x = \frac{1}{N}\sum_{i=0}^{N-1}|x[i]|^2$ is the average instantaneous subcarrier power within the OFDM symbol.

PAPR reduction techniques can be divided into two main categories [24], [26]. The first is distortionless techniques, which are applied prior to the IFFT stage. The second is signal distortion techniques, which are applied after the IFFT stage. Any PAPR technique presents a trade-off between a set of main performance parameters, namely: PAPR, BER, spectral efficiency and computational complexity. We discuss the trade-offs associated with the most notable of those techniques next.

### 1) DISTORTIONLESS TECHNIQUES

Several works proposed PAPR reduction by encoding the input data of the OFDM modulator in a manner that ensures avoiding codewords that cause high PAPR. Examples include using simple odd parity code [34], where a parity-check bit is used with group of information bits to create low PAPR codewords. The smaller the number of information bits, the more effective PAPR reduction, and the less spectral efficient the system will become. Similarly, in complement block/sub-block coding [35], [36], a complementary sequence of bits inserted within each data block to reduce PAPR. Golay complementary sequences were used in a similar manner in [37]. Although these methods can effectively reduce PAPR, they have very low spectral efficiency due to insertion of redundant bits or sequences. In addition, they introduce additional complexity due to the decoding process at the receiver.

Selective Mapping (SLM) techniques are based on multiplying the input data to the IFFT block to a set of different phase sequences, and then computing their IFFT simultaneously. The PAPR of each sequence is evaluated, and the one with lowest PAPR is selected for transmission [38]–[41]. SLM has the advantage of not introducing any distortion to the OFDM waveform, in addition to effectively reducing PAPR by about 2-4 dB, depending on the number of phase sequences used. However, it incurs added complexity due to the extra IFFT and PAPR calculations incurred by each phase sequence. In addition, the index of the selected phase sequence must be transmitted as side information to the receiver, which reduces spectral efficiency. In addition, due to the extreme sensitivity of operation to the side information, it is usually channel coded to ensure its reliability. This further reduces spectral efficiency. Some attempts were made to reduce SLM complexity [42]–[44], and to avoid using side information [45]–[47].

Partial Transmit Sequence (PTS) technique can be considered as an extension of SLM, yet with higher PAPR reduction capability [48], [49]. The technique is based on dividing the input data sequence into a set of non-overlapping sub-sequences, and apply IFFT to each of them independently. The outputs are scaled and phase rotated by a set of different values, and the combination that yields the least PAPR is chosen for transmission. Clearly, the complexity of PTS sequence increases drastically with the number of sub-sequences. In addition, similar to SLM, transmission of side information bits is required. A comparable method to SLM and PTS is called Dummy Sequence Insertion (DSI) [50], where a sequence is added to the input data to the IFFT block. This sequence is designed to reduce the output PAPR. This technique has closed loop feedback structure, where PAPR is calculated and compared to a target value at the output, and if it exceeds it, the process is repeated using another sequence. This technique is less complex than PTS, yet performs worse in terms of PAPR reduction.

Tone Reservation technique allocates a group of subcarriers (tones) from the OFDM system for PAPR reduction [51], [52]. Specialized algorithms are used to solve the optimization problem of finding the values of these subcarriers that can minimize PAPR [53]. While the PAPR reduction capability of this method is quite decent, a portion of subcarriers is no more transmitting information, leading to a considerable drop in data rate. In addition, calculating the optimum values carried by the reserved tones is quite complicated, which adds a computational burden to the transmitter [53], [54].

### 2) SIGNAL DISTORTION TECHNIQUES

Signal distortion techniques reduce PAPR by modifying signal shape post IFFT stage, which is far less complex than distortion-less techniques. However, they introduce a considerable drop in error performance. The most straightforward approach is clipping the peaks that exceed a certain hard or soft threshold [55]. While this approach is highly effective in PAPR reduction, it considerably increases transmission BER due to the distortion caused to the signal, in addition to the emergence of non-linear distortion caused by clipping, which leads to out-of-band interference. Peak windowing [56], adopts a similar approach by subjecting the OFDM sequence to a correcting time-domain window function such as Hamming, Kaiser and cosine windows. This also leads to considerable reduction of PAPR, at the cost of increased transmission error rate and out-of-band interference. Out-of-band interference is usually treated by post-filtering, which leads to peak regrowth. Iterative clipping

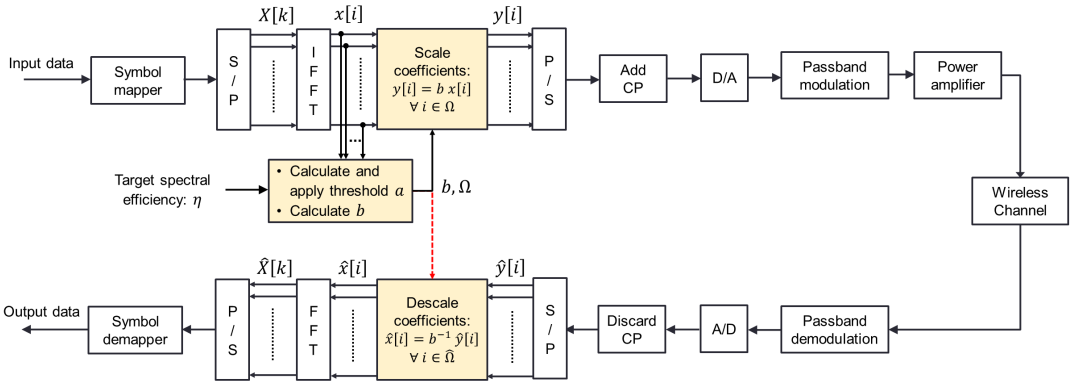


**FIGURE 2.** Block diagram of the OFDM transmitter and receiver incorporating the proposed technique.

and filtering performs several iterations of peak clipping and filtering until a satisfactory PAPR is achieved [57]–[62]. However, this comes at the cost of increasing computational complexity and implementation cost, besides the poor BER performance.

Companding techniques [63] borrow algorithms that are used in speech processing such as A-law and $\mu$-law algorithms for compressing the OFDM signal, which consequently reduces its PAPR. The process is reversed at the receiver by applying the inverse transformation (expanding the signal) without the need for transmission of side information. Companding methods use either linear transforms or non-linear transforms [64]–[66]. Linear companding has very low complexity with humble PAPR reduction capability. On the other hand, non-linear companding improves PAPR reduction capability at the cost of increasing computational complexity, further degrading BER performance and the emergence of out-of-band interference [26], [67]. In general, companding techniques cause significant rise in transmission error rate, which may not compensate for the PAPR reduction achieved in most cases. Recently, optimization techniques were used in [68] to design optimal companders with improved out-of-band power rejection performance.

To sum up the previous discussion, signal distortion techniques are effective in PAPR reduction and far less complex than distortionless techniques. However, their main drawback is that they have an upper bound on transmission error performance, i.e. most techniques cannot reach arbitrarily low BER at any SNR, which forces the system designer to limit modulation order and/or use low-rate channel coding, even if the channel SNR was high. This ultimately results in reducing the effective data transmission rate. In addition, due to the complexity of transmission error analysis, most literature lack a sufficiently rigorous error analysis, which hurdles efficient design of the system and link budgeting.

On the other hand, the high computational complexity of distortionless techniques represent a major disadvantage, especially for future very-high speed systems that target very high data rate, and employ very large FFT length such as LTE which supports up to 2048 subcarriers [7], DVB-T2 which is planned to support up to 32K subcarriers [12], and possibly other 5G systems that will be based on OFDM [15], [16]. Consequently, this will imply a very large number of computations that may add delays and contribute significantly to overall system power consumption. In this paper, we aim to introduce a very low complexity distortion PAPR reduction technique that has minimal effect on BER performance, and provides the designer with high flexibility to control the trade-off between PAPR reduction and spectral efficiency, according to system requirements and operation conditions.

## III. PROPOSED TECHNIQUE

Based on our review of the PAPR reduction techniques in the previous section, our design aims to control and optimize the trade-off between the three main parameters involved in the OFDM reduction process, namely, PAPR, level of distortion, and the amount of side information sent from the transmitter to the receiver. The main objective is to achieve a PAPR reduction that can compensate for any distortion caused to the OFDM waveform, and yet maintain a considerable overall gain. In addition, we aim to minimize computational complexity, which is highly essential feature, especially for battery operated and IoT devices.

Fig. 2 illustrates a block diagram of the OFDM transmitter and receiver incorporating blocks relevant to the proposed technique. The proposed technique is based on measuring the magnitudes of the time-domain coefficients at the output of the OFDM modulator, then replacing the coefficients whose magnitudes exceed a certain threshold ($a$) by a scaled version of themselves, where the scaling factor is $b$. The indices of the scaled coefficients and $b$ are transmitted to the receiver as side information to enable the receiver to reverse the process and restore the original coefficients. This process is designed in a manner that achieves maximum achievable PAPR reduction, and a controllable level of distortion in an AWGN channel, as to be discussed in the forthcoming sections.

The first challenge to be addressed is how to select the threshold and scaling factor in a manner that maintains an

optimal balance between minimizing PAPR, and minimizing distortion that may be incurred due to scaling/descaling in presence of additive noise. Suppose we subject the magnitudes of the entries of $x[i]$ to a threshold $a$, where all entries that exceed this threshold are linearly scaled by a factor $b$. The outcome $y[i]$ of this operation can be expressed as:

$$y[i] = \begin{cases} bx[i], & |x[i]| > a \\ x[i], & |x[i]| \leq a \end{cases} \tag{3}$$

for $i = 0, 1, \ldots, N-1$. The coefficients $x[i]$ are generally modeled as iid zero-mean complex Gaussian random variables [24]:

$$\begin{aligned} \Re\{x[i]\} &\sim \mathcal{N}\left(0, \frac{\sigma_x^2}{2}\right) \\ \Im\{x[i]\} &\sim \mathcal{N}\left(0, \frac{\sigma_x^2}{2}\right) \end{aligned} \tag{4}$$

where $\sigma_x^2$ is the variance of $x[i]$ and it is equal to $p_x$ since it has a zero mean. The above model is accurate for moderately large $N$ ($N \geq 256$), since the central-limit theorem holds strongly. Therefore, $|x[i]| = \sqrt{\Re\{x[i]\}^2 + \Im\{x[i]\}^2}$ is Rayleigh-distributed with uniform phase: $|x[i]| \sim \text{Rayleigh}(\sigma_x/\sqrt{2})$ [39], [69]. To simplify forthcoming analysis, let us define the following normalized variable:

$$u_i := \frac{|x[i]|}{\sigma_x} \tag{5}$$

Consequently, $u_i \sim \text{Rayleigh}(1/\sqrt{2})$ with the following probability density function (pdf) and cumulative distribution function (cdf) respectively:

$$\begin{aligned} f(u_i) &= 2u_i e^{-u_i^2} \\ F(u_i) &= 1 - e^{-u_i^2} \end{aligned} \tag{6}$$

Define a set $\Omega$ that includes the indices of the coefficients to be modified, and its complement set as follows:

$$\Omega = \{i : |x[i]| > a\}, \quad \text{and } \Omega^{\complement} = \{i : |x[i]| \leq a\} \tag{7}$$

The average number of elements in this set can hence be expressed as

$$N_a = \mathbb{E}(|\Omega|) = N \Pr(|x[i]| > a) = Ne^{-\alpha} \tag{8}$$

where

$$\alpha = \frac{a^2}{\sigma_x^2}$$

represents the normalized threshold, and

$$\Pr(|x[i]| > a) = \Pr(u_i > \sqrt{\alpha}) = 1 - F(\sqrt{\alpha}) = e^{-\alpha}$$

Thus, we may define the following probabilities:

$$\begin{aligned} P_{\Omega} &= \Pr(i \in \Omega) = e^{-\alpha} \\ P_{\Omega^{\complement}} &= \Pr(i \in \Omega^{\complement}) = 1 - e^{-\alpha} \end{aligned} \tag{9}$$

Finally, the cyclic prefix is added to $y[i]$, and fed to the digital-to-analog converter to proceed for passband modulation, power amplification, then transmission, as illustrated in Fig. 2. After the threshold-based scaling process described above, the indices of the scaled subcarriers are binary encoded, modulated, and transmitted to the receiver independently as side information, as to be discussed in the next section.

At the receiver side, and assuming an AWGN channel, the received baseband signal is expressed as follows:

$$\hat{y}[i] = y[i] + n[i] = \begin{cases} bx[i] + n[i], & i \in \Omega \\ x[i] + n[i], & i \in \Omega^{\complement} \end{cases} \tag{10}$$

We define the Transmission Signal to Noise Ratio (TSNR) at the input of the receiver as:

$$\gamma_t := \frac{\sigma_y^2}{\sigma_n^2} \tag{11}$$

where $\sigma_y^2$ and $\sigma_n^2$ are the variances of $y[i]$ and $n[i]$ respectively. In order to restore the original coefficients, the receiver uses the received side information bits to generate the index set $\hat{\Omega}$, which may not be exactly equal to the original $\Omega$, due to transmission errors. Based on $\hat{\Omega}$, the scaling process in (3) is reversed to give:

$$\hat{x}[i] = \begin{cases} b^{-1}\hat{y}[i], & i \in \hat{\Omega} \\ \hat{y}[i], & i \in \hat{\Omega}^{\complement} \end{cases} \tag{12}$$

## IV. PERFORMANCE ANALYSIS

The proposed technique is based on applying threshold-based scaling to the entries of the time-domain signal $x[i]$ at the output of IFFT block. The entries of $x[i]$ whose magnitude exceed a threshold $a$ are scaled by a factor $b$. The resulting signal is $y[i]$, which is modulated and transmitted instead of $x[i]$. Finally, the indices of the scaled entries are binary-encoded and transmitted to the receiver as side information. In this section, we analyze the impact of applying this technique on the three main performance metrics; namely PAPR, distortion and spectral efficiency.

### A. PAPR ANALYSIS

Based on the above discussion, we start by calculating the PAPR of $y[i]$, which we define as follows:

$$\rho_y := \frac{\max\limits_i \{|y[i]|^2\}}{\sigma_y^2} \tag{13}$$

where $\sigma_y^2 = \frac{1}{N}\sum_{i=0}^{N-1} |y[i]|^2$. The numerator of the above fraction can be evaluated by referring to (3), yielding

$$\max_i \{|y[i]|^2\} = \begin{cases} b^2 \max\limits_i \{|x[i]|^2\}, & a \leq b \max\limits_i \{|x[i]|\} \\ a^2, & a > b \max\limits_i \{|x[i]|\} \end{cases} \tag{14}$$

On the other hand, by using (3), (5) and (8), the denominator is evaluated as follows:

$$\begin{aligned}\sigma_y^2 &= \frac{1}{N}\left[b^2\sum_{i\in\Omega}|x[i]|^2+\sum_{i\in\Omega^{\complement}}|x[i]|^2\right]\\ &= \frac{\sigma_x^2}{N}\left[b^2\sum_{i\in\Omega}u_i^2+\sum_{i\in\Omega^{\complement}}u_i^2\right]\\ &= \sigma_x^2\left[b^2\,P_{\Omega}\mathbb{E}_{i\in\Omega}(u_i^2)+P_{\Omega^{\complement}}\mathbb{E}_{i\in\Omega^{\complement}}(u_i^2)\right]\\ &= \sigma_x^2\left[b^2\,e^{-\alpha}\mathbb{E}_{i\in\Omega}(u_i^2)+(1-e^{-\alpha})\mathbb{E}_{i\in\Omega^{\complement}}(u_i^2)\right] \quad (15)\end{aligned}$$

where $\mathbb{E}_{i\in\Omega}(\cdot)$ and $\mathbb{E}_{i\in\Omega^{\complement}}(\cdot)$ denote the expectation over the sets $\Omega$ and $\Omega^{\complement}$ respectively, and are given by:

$$\begin{aligned}\mathbb{E}_{i\in\Omega}(u_i^2) &= 1+\alpha\\ \mathbb{E}_{i\in\Omega^{\complement}}(u_i^2) &= \frac{1-e^{-\alpha}(1+\alpha)}{1-e^{-\alpha}} = \frac{1-c_0}{1-e^{-\alpha}} \quad (16)\end{aligned}$$

where

$$c_0 = e^{-\alpha}(1+\alpha)$$

The detailed derivation of the above expressions is given in Appendix.

From the two above equations, and after some rearrangement, we may write the ratio between $\sigma_y^2$ and $\sigma_x^2$ as follows:

$$\lambda = \frac{\sigma_y^2}{\sigma_x^2} = 1-e^{-\alpha}(1+\alpha)(1-b^2) = 1-c_0(1-b^2) \quad (17)$$

Therefore, by applying (2), (14) and (17) to (13), we may express $\rho_y$ in terms of $\alpha$, $b$ and $\rho_x$ as follows:

$$\rho_y = \begin{cases}\dfrac{b^2\rho_x}{\lambda}, & 0<\alpha\le b^2\rho_x\\ \dfrac{\alpha}{\lambda}, & \alpha > b^2\rho_x\end{cases} \quad (18)$$

### B. DISTORTION ANALYSIS

In this section we aim to evaluate the error performance of the proposed method in terms of the Normalized Mean-Squared Error (NMSE) between the original modulated sequence $x[i]$ and the recovered sequence $\hat{x}[i]$. The NMSE is defined as:

$$\text{NMSE} := \frac{\mathbb{E}(|x[i]-\hat{x}[i]|^2)}{\sigma_x^2} \quad (19)$$

The recovery process at the receiver mainly relies on the scaled coefficients' indices transmitted via side information bits, which are not expected to be received error-free. Thus, we start by defining two sets of successfully estimated indices as follows:

$$\begin{aligned}\mathcal{S}_1 &= \{i : i\in\hat{\Omega}^{\complement}\cap\Omega^{\complement}\}\\ \mathcal{S}_2 &= \{i : i\in\hat{\Omega}\cap\Omega\} \quad (20)\end{aligned}$$

On the other hand, for the case of erroneous transmission of scaled indices, we define the two following sets:

$$\begin{aligned}\mathcal{E}_1 &= \{i : i\in\hat{\Omega}\cap\Omega^{\complement}\}\\ \mathcal{E}_2 &= \{i : i\in\hat{\Omega}^{\complement}\cap\Omega\} \quad (21)\end{aligned}$$

where $\mathcal{E}_1$ represents the set of indices originally in $\Omega^{\complement}$, but erroneously decided to be in $\hat{\Omega}$, and vice versa for $\mathcal{E}_2$. Thus, coefficients in $\mathcal{E}_1$ will be erroneously scaled by $b^{-1}$, while those in $\mathcal{E}_2$ will not be scaled, although they actually should be. Consequently, we can rewrite (12) as:

$$\hat{x}[i] = \begin{cases}x[i]+n[i], & i\in\mathcal{S}_1\\ x[i]+b^{-1}n[i], & i\in\mathcal{S}_2\\ b^{-1}x[i]+b^{-1}n[i], & i\in\mathcal{E}_1\\ bx[i]+n[i], & i\in\mathcal{E}_2\end{cases} \quad (22)$$

Without loss of generality, we assume that the side information bits are mapped by MQAM with order $M_s$ with no channel coding and transmitted independently from the data payload. Thus, the symbol error probability over an AWGN channel assuming a square constellation (i.e. $M_s = 4, 16, 64, \ldots$) is given by [70]:

$$P_s = 1-\left(1-2\frac{\sqrt{M_s}-1}{\sqrt{M_s}}Q\left(\sqrt{\frac{3\gamma_t}{M_s-1}}\right)\right)^2 \quad (23)$$

Consequently, since each scaled index is encoded into a $\log_2 N$ bits word, the worst-case probability of word error (i.e. assuming one error per word) is given by:

$$P_w = P_s\frac{\log_2(N)}{\log_2(M_s)} \quad (24)$$

where $Q(m) = 1/\sqrt{2\pi}\cdot\int_m^{\infty}\exp(-r^2/2)\mathrm{d}r$ is the Q-function of the standard normal distribution.

Each erroneous estimated index caused by a word error may point to an index in $\Omega$ with probability $P_{\Omega}$, or point to an index in $\Omega^{\complement}$ with probability $P_{\Omega^{\complement}} = 1-P_{\Omega}$. Consequently, the probability that an index $i$ falls in $\mathcal{E}_1$ is given by:

$$\begin{aligned}P_{\mathcal{E}_1} &= \Pr(i\in\mathcal{E}_1)\\ &= \Pr(i\in\Omega^{\complement}\mid i\in\hat{\Omega})\Pr(i\in\hat{\Omega})\\ &= P_wP_{\Omega^{\complement}}P_{\Omega} = P_w(1-e^{-\alpha})e^{-\alpha} \quad (25)\end{aligned}$$

where in this case, an erroneous index pointed to an index that originally belongs to $\Omega^{\complement}$, which occurs with probability $P_wP_{\Omega^{\complement}}$. On the other hand, the probability that an index $i$ falls in $\mathcal{E}_2$ is given by:

$$\begin{aligned}P_{\mathcal{E}_2} &= \Pr(i\in\mathcal{E}_2)\\ &= \Pr(i\in\hat{\Omega}^{\complement}\mid i\in\Omega)\Pr(i\in\Omega)\\ &= P_wP_{\Omega} = P_we^{-\alpha} \quad (26)\end{aligned}$$

where in this case, the index error led to missing a member of $\Omega$, which occurs inevitably whenever an index error takes place. Hence, this event occurs with probability $P_w$. Since the sets $\mathcal{S}_1, \mathcal{S}_2, \mathcal{E}_1, \mathcal{E}_2$ are mutually exclusive, and $\mathcal{S}_1+\mathcal{S}_2+\mathcal{E}_1+\mathcal{E}_2 = \{0, 1, \ldots, N-1\}$, therefore the probabilities of

correctly identifying scaled and unscaled sub-carriers can be written as:

$$\begin{aligned} P_{\mathcal{S}_1} &= \Pr(i \in \mathcal{S}_1) = P_{\Omega^{\complement}} - P_{\mathcal{E}_1} \\ &= (1 - e^{-\alpha})(1 - P_w e^{-\alpha}) \end{aligned} \tag{27}$$

and

$$\begin{aligned} P_{\mathcal{S}_2} &= \Pr(i \in \mathcal{S}_2) = P_{\Omega} - P_{\mathcal{E}_2} \\ &= e^{-\alpha}(1 - P_w) \end{aligned} \tag{28}$$

From the above analysis, we can express the mean squared error between the transmitted signal $x[i]$ and the recovered signal at the receiver $\hat{x}[i]$ in (22) as follows:

$$\begin{aligned} &\mathbb{E}(|x[i] - \hat{x}[i]|^2) \\ &\quad = P_{\mathcal{S}_1}\sigma_n^2 + P_{\mathcal{S}_2} b^{-2}\sigma_n^2 \\ &\qquad + P_{\mathcal{E}_1}\left[\mathbb{E}_{i\in\Omega^{\complement}}\left((b^{-1}-1)^2 x^2[i]\right) + b^{-2}\sigma_n^2\right] \\ &\qquad + P_{\mathcal{E}_2}\left[\mathbb{E}_{i\in\Omega}\left((b-1)^2 x^2[i]\right) + \sigma_n^2\right] \end{aligned} \tag{29}$$

By applying (16) and (25) to (28), and performing some simplifications and rearrangement, we reach:

$$\begin{aligned} &\mathbb{E}(|x[i] - \hat{x}[i]|^2) \\ &\quad = \sigma_x^2 P_w\left[e^{-\alpha}(b^{-1}-1)^2(1-c_0) + c_0(b-1)^2\right] \\ &\qquad + \sigma_n^2\left[1 - e^{-\alpha}(1 - P_w e^{-\alpha})) + b^{-2}e^{-\alpha}(1 - P_w e^{-\alpha})\right] \\ &\quad = \sigma_x^2 P_w e^{-\alpha}(b^{-1}-1)^2(1 + c_0(e^{\alpha}b^2 - 1)) \\ &\qquad + \sigma_n^2\left[1 + e^{-\alpha}(b^{-2}-1)(1 - P_w e^{-\alpha})\right] \end{aligned} \tag{30}$$

The above expression can be further simplified by observing that the term $P_w e^{-\alpha}$ is negligible, since $P_w \ll 1$ for any moderate TSNR, and $e^{-\alpha} \ll 1$ since it is expected that $\alpha > 3$ for proper system operation, as to be deduced in Section V. Thus the product of the two terms will be extremely small, and can be safely omitted without any loss of precision. Consequently, the NMSE defined in (19) can be expressed as:

$$\begin{aligned} \text{NMSE} = P_w e^{-\alpha}(b^{-1}-1)^2\left(1 + c_0(e^{\alpha}b^2 - 1)\right) \\ + \frac{\lambda}{\gamma_t}\left(1 + e^{-\alpha}(b^{-2}-1)\right) \end{aligned} \tag{31}$$

### C. SPECTRAL EFFICIENCY

Transmission of side information will lead to either reducing the transmission data rate if bandwidth is fixed, or requiring extra bandwidth. Without loss of generality, we assume that the system is assigned a fixed bandwidth, and hence transmission of side information will reduce the data rate. Suppose the original transmission symbol rate without transmission of any side information is $R = N/T$, where $T$ is the OFDM symbol duration. On the other hand, upon transmission of side information at a symbol rate $R_s$, data will be transmitted at symbol rate $R_d = R - R_s$. We hence define the system spectral efficiency as:

$$\eta := \frac{R_d}{R} = 1 - \frac{R_s}{R} \tag{32}$$

From (8), we need to encode and transmit an average of $N_a$ indices as side information for each OFDM symbol, i.e. every $T$ seconds. To simplify expressions, we neglect the bits required to encode $b$, since they are very few compared to those required for encoding the peak indices. Since encoding each peak index requires $\log_2 N$ bits, and assuming that side information symbols are mapped by MQAM with order $M_s$, then $R_s$ can be expressed as:

$$R_s = \frac{N_a}{T}\frac{\log_2 N}{\log_2 M_s} = Re^{-\alpha}\frac{\log_2 N}{\log_2 M_s} \tag{33}$$

Consequently, the spectral efficiency can be expressed as:

$$\eta = 1 - e^{-\alpha}\frac{\log_2 N}{\log_2 M_s} \tag{34}$$

From (34), we can deduce that there is a strong dependency between spectral efficiency, $\alpha$ and $M_s$, which directly impacts data rate. This dependency is illustrated graphically in Fig. 3. This dependency and the trade-offs involved with it are discussed in the following section.

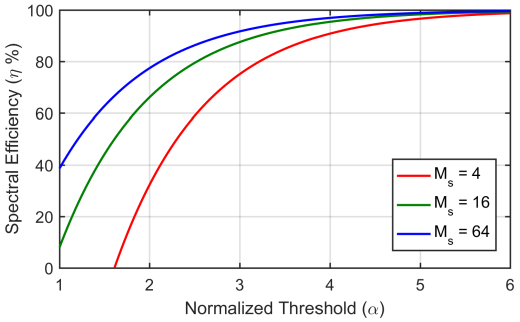


**FIGURE 3.** Spectral efficiency ($\eta$) versus normalized threshold ($\alpha$) for various values of $M_s$ at $N = 1024$.

## V. PARAMETER SELECTION AND OPTIMIZATION

### A. PARAMETER SELECTION

In this section, we present our choices of the parameters $\alpha$ and $b$, and discuss the resulting trade-off between PAPR, NMSE and spectral efficiency. Initially, the system designer selects an arbitrary target value of $\eta$ that complies with system specifications and operation conditions. Consequently, (34) is used to determine the normalized threshold $\alpha$ as follows:

$$\alpha^* = \log\left(\frac{\log_2 N}{(1-\eta)\log_2 M_s}\right) \tag{35}$$

On the other hand, from (18), we deduce that the value of the scaling factor $b$ has a direct impact on PAPR. Therefore it is highly desirable to select the optimum value of $b$ that minimizes $\rho_y$. By differentiating the expression of $\rho_y$ given in (18) with respect to $b$, we get:

$$\frac{\partial \rho_y}{\partial b} = \begin{cases} \dfrac{2b(1-c_0)\rho_x}{(c_0 b^2 - c_0 + 1)^2}, & b \geq \sqrt{\alpha/\rho_x} \\ \dfrac{-2c_0\alpha b}{(c_0(b^2-1)+1)^2}, & 0 < b < \sqrt{\alpha/\rho_x} \end{cases} \tag{36}$$

Keeping in mind that $0 \leq c_0 \leq 1 \, \forall \, \alpha \geq 0$, we can deduce that for any value of $b > 0$, the gradient of $\rho_y$ is strictly positive for $b \geq \sqrt{\alpha/\rho_x}$ (i.e. $\rho_y$ is monotonically increasing), and strictly negative for $0 < b < \sqrt{\alpha/\rho_x}$ (i.e. $\rho_y$ is monotonically decreasing). This implies that the optimum value of $b$ that minimizes $\rho_y$ occurs at the intersection of both curves.

We graphically illustrate this observation by plotting $\rho_y$ expressed in (18) versus $b$, as shown in Fig. 4 for various combinations of $\eta$ and $M_s$. We observe that the inflection point of the curves lies exactly at the optimum value of $b$ given by:

$$b^* = \sqrt{\frac{\alpha}{\rho_x}} \tag{37}$$

Consequently, $\rho_y$ in (18) can be re-written as:

$$\rho_y = \frac{\alpha}{1 - c_0(1 - \frac{\alpha}{\rho_x})} \tag{38}$$

where $c_0 = e^{-\alpha}(1 + \alpha)$. In addition, we observe from Fig. 4 that, as expected, higher spectral efficiency $\eta$ results in higher PAPR level. In addition, we observe that higher side information modulation order has a significant impact on reducing PAPR. However, before jumping to any conclusions from these observations, we have to investigate the impact of these parameters on signal distortion.

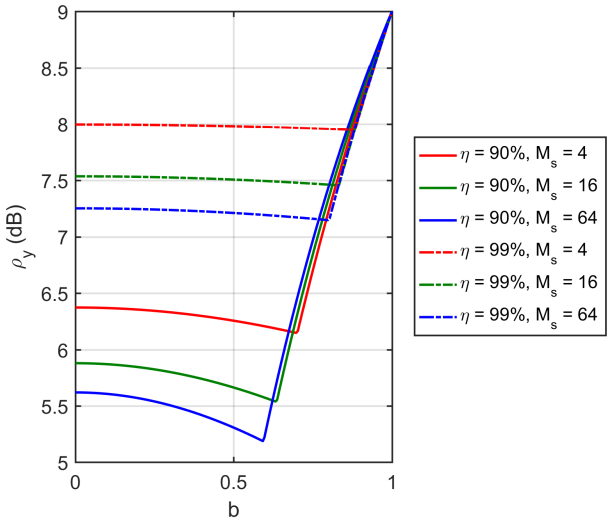


**FIGURE 4.** PAPR vs $b$ for $M_s = \{4, 16, 64\}$, $\eta = \{90\%, 99\%\}$, and $N = 1024$. The plots employ $\rho_x = 9$ dB, which is the average PAPR value calculated from Monte Carlo simulations.

In order to make our discussion of signal distortion more elaborate, we define Recovery SNR (RSNR) as follows:

$$\gamma_r := \frac{\sigma_x^2}{\mathbb{E}(|x[i] - \hat{x}[i]|^2)} = \frac{1}{\text{NMSE}} \tag{39}$$

By using (31), we compare the transmission SNR found at the input of the receiver to the SNR achieved after descaling the received coefficients $\hat{y}[i]$ and recovering $\hat{x}[i]$. This enables us to quantify the distortion caused by applying our proposed

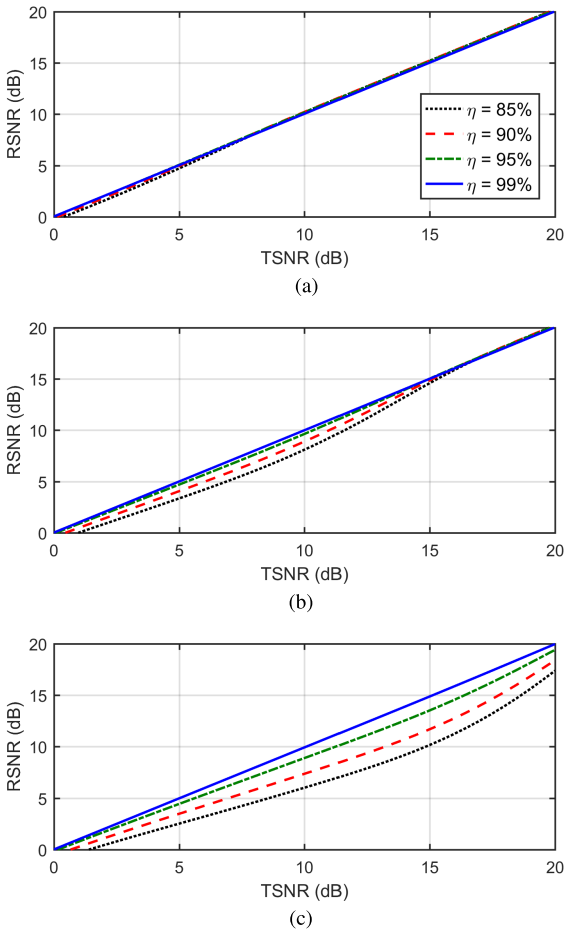


**FIGURE 5.** RSNR versus TSNR for various values of $\eta$ and $M_s$ at $N = 1024$. (a) $M_s = 4$. (b) $M_s = 16$. (c) $M_s = 64$.

technique in the presence of additive noise. Fig. 5 illustrates the RSNR versus TSNR at various target spectral efficiency $\eta = \{85\%, 90\%, 95\%, 99\%\}$ for three cases, namely $M_s = 4$, $M_s = 16$ and $M_s = 64$. We first observe that smaller $M_s$ corresponds to better RSNR for all values of $\eta$, which is logic, since smaller $M_s$ result in a lower probability of error in side information transmission. We also observe that for all values of $M_s$, increasing $\eta$ results in a better RSNR. This is due to the fact that higher $\eta$ implies larger threshold $\alpha$ and hence less scaled subcarriers, which leads to a smaller drop in RSNR. By comparing observations from Fig. 4 and Fig. 5, we find that increasing $\eta$ results in a worse PAPR, but better RSNR. The same applies to decreasing $M_s$. Hence, we need to make the best trade-off by making an optimal choice of $M_s$ for a given $\eta$ that provide maximum overall performance improvement. This can be achieved by employing an objective function that considers both PAPR and RSNR, as to be discussed next.

### B. METHOD GAIN

Previous works on signal distortion PAPR reduction techniques such as peak clipping, windowing and companding focused on the PAPR reduction aspect of their techniques,

without rigorous analytic quantification of the performance penalty due to distortion, which directly impacts BER performance [57]–[66]. In Section IV, we have discussed the impact of our proposed technique on reducing PAPR, and on the level of distortion it may introduce due to the effect of additive noise in terms of RSNR. In this section, we identify the extent to which the proposed method is effective by evaluating the net gain it can achieve. Although PAPR reduction enables shifting the operating point of the transmitter's power amplifier, and hence increasing the TSNR, distortion leads to a drop in RSNR, which directly degrades BER. Therefore, a portion of the SNR gain achieved by PAPR reduction will be deducted in order to maintain the BER performance of the original signal prior to applying PAPR reduction. This concept can be applied for evaluating any PAPR reduction technique. In mathematical terms, the net gain achieved by our proposed method can be expressed in dB terms as follows:

$$(G)_{\text{dB}} = \left[(\rho_x)_{\text{dB}} - (\rho_y)_{\text{dB}}\right] - \left[(\gamma_t)_{\text{dB}} - (\gamma_r)_{\text{dB}}\right] \quad (40)$$

where $(r)_{\text{dB}} = 10\log_{10}(r)$. Hence a PAPR reduction technique is considered effective if $(G)_{\text{dB}} > 0$ dB. By switching to ratio terms, and using (37), (38) and (39), we can rewrite the above expression after some rearrangements as follows:

$$G = \frac{\rho_x}{\rho_y} \times \frac{\gamma_r}{\gamma_t} = \frac{\rho_x \lambda}{K} \quad (41)$$

where

$$K = \gamma_t P_w e^{-\alpha}(\sqrt{\rho_x} - \sqrt{\alpha})^2(1 + c_0(e^{\alpha}\alpha/\rho_x - 1)) + \lambda(\alpha + e^{-\alpha}(\rho_x - \alpha))$$

$$P_w = \frac{\log_2(N)}{\log_2(M_s)}\left[1 - \left(1 - 2\frac{\sqrt{M_s}-1}{\sqrt{M_s}}Q\left(\sqrt{\frac{3\gamma_t}{M_s - 1}}\right)\right)^2\right]$$

$$\alpha = \log\left(\frac{\log_2 N}{(1-\eta)\log_2 M_s}\right)$$

$$c_0 = e^{-\alpha}(1+\alpha)$$

$$\lambda = 1 - e^{-\alpha}(1+\alpha)(1-\alpha/\rho_x)$$

We can deduce from the above expression that the net gain is a function of a set of parameters; some of which are uncontrollable, namely TSNR ($\gamma_t$), original data PAPR ($\rho_x$) and OFDM symbol length ($N$). On the other hand, controllable parameters are the target spectral efficiency ($\eta$) and side information modulation order ($M_s$). These two parameters determine the value of the normalized threshold ($\alpha$).

As discussed in the previous subsection, for a given value of $\eta$, we have a trade-off between increasing $M_s$ to maximize PAPR reduction, and decreasing $M_s$ to minimize distortion. Examining the net gain for various values of $M_s$ enables us to solve this trade-off. Fig. 6 illustrates the values of net gain in dB versus TSNR for various values of $M_s$ at $\eta = \{90\%, 95\%, 99\%\}$. We observe that the maximum net gain is achieved at $M_s = \{8, 16\}$, $M_s = 16$ and $M_s = 64$ for $\eta = 90\%$, $\eta = 95\%$ and $\eta = 99\%$, respectively. Hence, we may conclude that higher modulation order provide higher net gain for high values of target spectral efficiency.

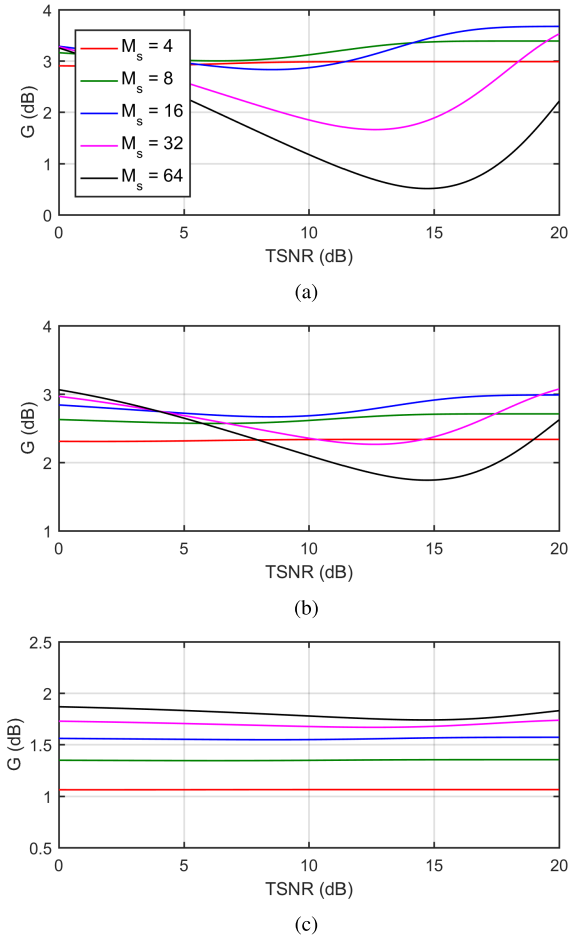


**FIGURE 6.** Net gain in dB versus TSNR in dB for various values of modulation order $M_s$, and spectral efficiency $\eta$, at $N = 1024$. (a) $\eta = 90\%$. (b) $\eta = 95\%$. (c) $\eta = 99\%$.

To further investigate this issue, Fig. 7 illustrates the values of $(G)_{\text{dB}}$ versus $\eta$ at $M_s = \{16, 64\}$. We observe that higher gain is achieved by $M_s = 64$ if $\eta$ exceeds about 97%. In addition, we observe that a higher TSNR results in a higher net gain. In general, this figure provides us with an overview of the net gain achievable at a given value of target $\eta$, and provides a visual confirmation that the proposed technique is capable of providing a considerable net gain for any value of spectral efficiency, even if it was as high as 99%. Therefore, (41) can be used by the system designer to optimize system parameters in order to grant maximum achievable gain.

## VI. MECHANISM OPERATION AND COMPLEXITY ANALYSIS

The overall operation of the proposed method in implementation level is modeled in two algorithms shown in Fig. 8 for the transmitter, and Fig. 8b for the receiver. We assume that initially, the transmitter and receiver have agreed on a target spectral efficiency $\eta$. The transmitter should store a lookup table that includes the values of the normalized threshold: $\alpha^*$ calculated from (35) for given values of $\eta$, $N$ and $M_s$.

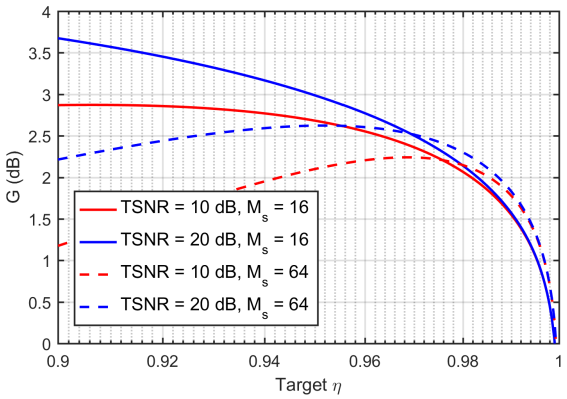


**FIGURE 7.** Net gain in dB versus target spectral efficiency for $N = 1024$, $M_s = \{16, 64\}$.

**Input:** Target spectral efficiency: $\eta$, OFDM symbol length: $N$, side information modulation order: $M_s$ and OFDM sequence: $x[i]$.

**Output:** Shaped OFDM sequence: $y[i]$.

1) **Set main parameters:**
   - Look up $\alpha^* = \log\left(\frac{\log_2 N}{(1-\eta)\log_2 M_s}\right)$
   - Calculate $\sigma_x^2 = \frac{1}{N}\sum_{i=0}^{N-1}|x[i]|^2$
   - Calculate $x_{\max} = \max_i\{|x[i]|\}$
   - Calculate $a^2 = \alpha^*\sigma_x^2$ and $b = a/x_{\max}$
2) **Threshold-based coefficients regulation:**
   **for** $i = 0 : N-1$
   **if** $|x[i]|^2 > a^2$,
   $y[i] = b\,x[i]$
   **else**
   $y[i] = x[i]$
3) **Output:** Return $y[i]$

(a)

**Input:** Recovered scaled index set: $\hat{\Omega}$, scaling coefficient: $b$, and received OFDM sequence: $\hat{y}[i]$.

**Output:** Recovered OFDM sequence: $\hat{x}[i]$.

1) **Set main parameters:**
   - Calculate $b^{-1}$
2) **Coefficients regulation:**
   **for** $i \in \hat{\Omega}$
   $\hat{x}[i] = b^{-1}\,\hat{y}[i]$
3) **Output:** Return $\hat{x}[i]$

(b)

**FIGURE 8.** An algorithmic description of the proposed technique at the transmitter and receiver. (a) Transmitter algorithm. (b) Receiver algorithm.

Table 1 provides an exemplary look-up table to be used by the transmitter for determining $\alpha^*$.

The transmitter algorithm is composed of two main stages.

**TABLE 1.** List of values of $\alpha^*$ corresponding to different values of $N$, $M_s$ and $\eta$. This table represents an exemplary lookup table to be used by the transmitter for calculating the appropriate value of $\alpha^*$.

| $N$ | $M_s$ | $\eta = 85\%$ | $\eta = 90\%$ | $\eta = 95\%$ | $\eta = 98\%$ |
|---|---|---|---|---|---|
| 256 | 4 | 3.2834 | 3.6889 | 4.3820 | 5.2983 |
| 256 | 16 | 2.5903 | 2.9957 | 3.6889 | 4.6052 |
| 256 | 64 | 2.1848 | 2.5903 | 3.2834 | 4.1997 |
| 512 | 4 | 3.4012 | 3.8067 | 4.4998 | 5.4161 |
| 512 | 16 | 2.7081 | 3.1135 | 3.8067 | 4.723 |
| 512 | 64 | 2.3026 | 2.7081 | 3.4012 | 4.3175 |
| 1024 | 4 | 3.5066 | 3.912 | 4.6052 | 5.5215 |
| 1024 | 16 | 2.8134 | 3.2189 | 3.9120 | 4.8283 |
| 1024 | 64 | 2.4079 | 2.8134 | 3.5066 | 4.4228 |
| 2048 | 4 | 3.6019 | 4.0073 | 4.7005 | 5.6168 |
| 2048 | 16 | 2.9087 | 3.3142 | 4.0073 | 4.9236 |
| 2048 | 64 | 2.5033 | 2.9087 | 3.6019 | 4.5182 |

In the first stage, after looking up $\alpha^*$, the transmitter calculates $\sigma_x^2$ and $x_{\max}$, and uses them to calculate $a^2$ and $b$. In the second stage, entries of the transmit data sequence $x[i]$ whose squared magnitudes exceed $a^2$ are scaled by $b$. We prefer to use the squared absolute value rather than absolute value described in (3), to avoid unnecessary square-root calculations. On the other hand, the receiver algorithm is essentially simpler; it starts by calculating the reciprocal of the scaling factor $b$, then calculating exactly $N_a = |\hat{\Omega}|$ multiplications.

Based on the two algorithms described above, the computational complexity of the proposed technique can be calculated in a straightforward manner. Step (1) in transmitter algorithm is dominated by the calculation of average instantaneous power $\sigma_x^2$, which requires $\mathcal{O}(N)$ computations. The remaining calculations are constant-time calculations, i.e. require $\mathcal{O}(1)$ computations. On the other hand, Step (2) of both algorithms also requires $\mathcal{O}(N)$ computations. Therefore, we may conclude that the proposed technique has a linear complexity in terms of the number of subcarriers $N$.

Table 2 lists a detailed analysis of the number and type of computations required by the proposed method for the

**TABLE 2.** A detailed analysis of the number of real arithmetic operations required for the transmitter and receiver algorithms.

| Quantity | $+$ | $\times$ | $\div$ | $\sqrt{\ }$ |
|---|---|---|---|---|
| $\sigma_x^2$ | $2N-1$ | $2N$ | 1 | 0 |
| $x_{\max}$ | 0 | 0 | 0 | 1 |
| $a^2$ | 0 | 1 | 0 | 0 |
| $b$ | 0 | 0 | 1 | 0 |
| $y[i]$ | 0 | $2N_a$ | 0 | 0 |
| $b^{-1}$ | 0 | 0 | 1 | 0 |
| $\hat{x}[i]$ | 0 | $2N_a$ | 0 | 0 |

transmitter and receiver. We highlight that since $x[i]$ is complex, hence calculating $|x[i]|^2 = \Re\{x[i]\}^2 + \Im\{x[i]\}^2$ requires two real multiplications and one real addition. Consequently, calculating $\sigma_x^2$ at the transmitter or $\sigma_y^2$ at the receiver would require $2N-1$ additions, $2N$ multiplications and one division, as shown in the tables. In addition, we highlight that Step (2) in transmitter algorithm does not require calculating $|x[i]|^2$, since the values calculated in Step (1) can be reused. Similarly, calculating $x_{\max}^2$ can be determined by sequentially updating the maximum value of $|x[i]|^2$. Hence, calculating $x_{\max}$ will require only one square root operation.

By adding up all computations, and assuming $N \gg 1$, we can reach the following approximation of the upper bound on the average number of real computations required by the transmitter and receiver:

$$\begin{aligned}\text{Number of TX computations} &\approx (4+2N_a)N \\ &= \left(4+2\frac{(1-\eta)\log_2 M_s}{\log_2 N}\right)N \\ &\leq \left(4+2\frac{\log_2 M_s}{\log_2 N}\right)N \qquad (42)\end{aligned}$$

and similarly,

$$\text{Number of RX computations} \leq 2\frac{\log_2 M_s}{\log_2 N}N \qquad (43)$$

The above expressions confirm that the computational complexity of our proposed technique is linear at the transmitter, and shows that it is sub-linear at the receiver. We hence may claim that the complexity of the proposed method is minimal compared to most other methods in literature. For example, the complexity analysis in [26] shows that clipping an filtering technique requires $\mathcal{O}(NL)$ operations, where $L$ is the Finite Impulse Response (FIR) filter length. On the other hand, SLM technique requires $\mathcal{O}(SN\log_2 N)$ operations, where $S$ is the number of phase sequences. Furthermore, PTS technique requires $\mathcal{O}(NP^2)$ operations, where $P$ is the number of partial sequences.

## VII. SIMULATION RESULTS AND DISCUSSION

In this section, we present simulated results for evaluating and comparing the performance of the proposed technique to other OFDM reduction techniques. Simulations are performed on a baseband model of the OFDM transmitter and receiver, which is based on the block diagram shown in Fig. 2. Transmission takes place over an AWGN channel, and without insertion of cyclic prefix. Randomly generated data bits are mapped by MQAM with order $M_d = 16$ and modulated by OFDM with $N = 1024$ subcarriers and no oversampling. Side information bits are similarly mapped by MQAM with order $M_s$. For a selected value of spectral efficiency ($\eta$), the values of $\alpha$ and $b$ are calculated using (35) and (37) respectively.

PAPR performance is most commonly evaluated by the Complementary Cumulative Distribution Function (CCDF) metric, which is defined as the probability that the OFDM signal PAPR ($\rho$) exceeds a given threshold ($\rho_0$). Hence, it can be expressed as follows:

$$\text{CCDF}(\rho_0) := \Pr(\rho > \rho_0) \qquad (44)$$

Fig. 9 illustrates the CCDF curves for the proposed technique compared to that of the original signal and a selection of other PAPR reduction techniques discussed in Section II. The curves shown for the proposed technique comprise $\eta = \{90\%, 95\%, 98\%, 99\%\}$ and $M_s = \{16, 16, 64, 64\}$ respectively. On the other hand, we show results achieved by selective mapping technique with $S = 8$ phase sequences [39], partial transmit sequence with $P = 8$ sub-sequences [49], peak clipping technique with peak power threshold given by $2.8p_x$ [71], and linear companding technique with transform function given by $C(x) = 0.8x + 0.1$ [67].

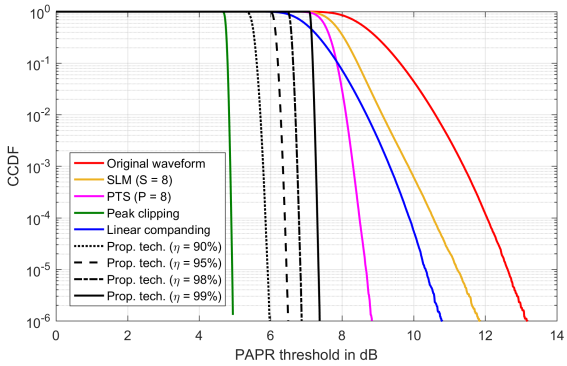


**FIGURE 9. CCDF comparison for the proposed technique and various other techniques at $N = 1024$.**

Initially, we observe that the proposed technique achieves significant reduction of PAPR compared to the original waveform, where PAPR does not exceed 6 dB for $\eta = 90\%$, 6.5 dB for $\eta = 95\%$, 6.9 dB for $\eta = 98\%$ and 7.4 dB for $\eta = 99\%$. These values agree with the analytic curves in Fig. 4. As compared to other techniques, the proposed technique outperforms all other examined techniques except for peak clipping technique, which has an obvious advantage in terms of PAPR reduction. However, this advantage does not apply for BER performance as to be shown shortly.

The steepness of the CCDF curves in Fig. 9 indicates very weak dependence of the PAPR of our proposed technique on the original PAPR, and hence the number of subcarriers $N$. This observation is predicted by the analytic expression in (38). We may also verify this observation by studying the curves shown in Fig. 10, which illustrate the CCDF curves for the proposed technique at $N = \{256, 512, 1024, 2048\}$ and $\eta = \{90\%, 95\%, 99\%\}$. We observe that the PAPR values are very slightly affected by increasing $N$, while the effect is more significant for the original waveform. This is highly advantageous for current and future high-speed wireless systems, which indeed seek maximizing the number of subcarriers $N$. For example, LTE standard supports up to 2048 subcarriers [7], while DVB-T2 is planned to support up to 32K subcarriers [12]. Keeping in mind the very low

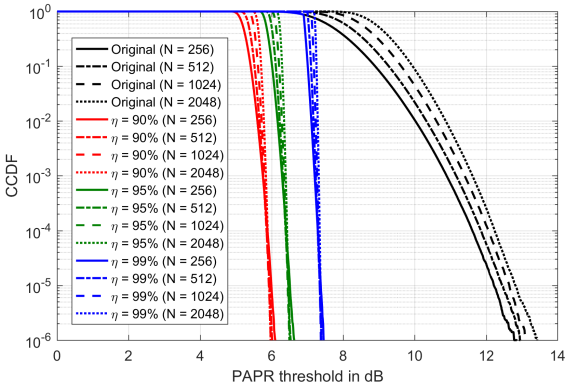


**FIGURE 10.** CCDF comparison for the proposed technique at $N = \{256, 512, 1024, 2048\}$ and $\eta = \{90\%, 95\%, 99\%\}$.

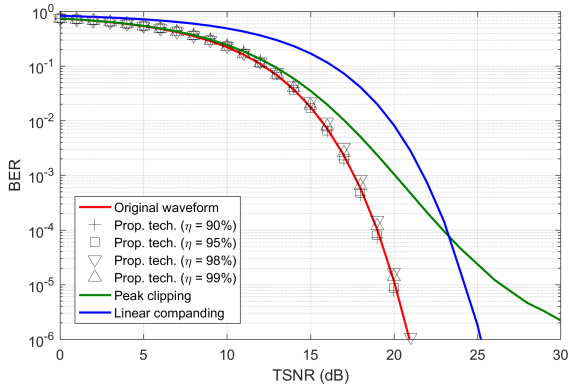


**FIGURE 11.** BER comparison for the proposed technique and various other techniques at $N = 1024$ and $M_d = 16$.

complexity of our proposed technique, we may conclude that the proposed technique could be ideal for such systems.

Fig. 11 compares BER performance versus SNR for the same set of PAPR reduction techniques in Fig. 9. In order to avoid cluttering the diagram, we omitted the curves of SLM and PTS techniques, since distortionless techniques do not impact BER by nature (assuming perfect side information transmission for these techniques). We observe that while the BER performance is minimally affected by applying our technique for all cases of $\eta$ shown, the performance of the signal distortion techniques (peak clipping and companding techniques) are significantly worse. This results in neutralizing the PAPR reduction advantage of these methods. For example, in order to achieve BER of $10^{-5}$, peak clipping and companding techniques require increasing the SNR by about 6.5 dB and 4.2 dB respectively, which counteracts the gain achieved by PAPR reduction.

It is worth mentioning that distortionless techniques also require transmission of side information, and that the overall performance of these techniques is very sensitive to the integrity of side information [26], [33]. Consequently, these data are usually protected by several layers of channel coding, which further degrades their spectral efficiency. The results shown in Fig. 11 for the technique were achieved while the side information bits were transmitted unprotected over the noisy channel. We may hence deduce that the proposed technique has a clear advantage over distortionless techniques in terms of robustness against noise, besides better PAPR reduction and less complexity.

## VIII. CONCLUSIONS

The PAPR reduction literature comprises numerous effective techniques. However, most commercial system implementations favor signal distortion techniques with affordable complexity such as iterative clipping and filtering, despite their negative impact on transmission BER [26], [71]. On the other hand, distortionless techniques suffer unrealistic computational complexity, especially upon employing a large number of subcarriers.

In this paper, we presented a PAPR reduction technique that maintains the effectiveness and simplicity of signal distortion techniques without degrading system BER. These gains are achieved in return for a slight (and controllable) reduction. However, we argue that although signal distortion techniques do not send side information, their degraded BER performance will probably entail applying channel coding in order to preserve the integrity of data. Hence, effectively, the data rate would be significantly reduced, in addition to the impact on computational complexity associated with the decoding process. On the other hand, we showed that the proposed technique is capable of achieving significant PAPR reduction, without BER degradation, even at 99% spectral efficiency, and without applying channel coding neither to data, nor to side information. Furthermore, since the proposed technique is based on linear scaling of coefficients, it does not suffer from the out-of-band interference caused by nonlinear signal shaping such as peak clipping and companding, and hence it does not require any iterative shaping/filtering processes.

Another main strength of this work is that it is supported by detailed analysis of the major performance criteria involved with the process. We showed via the notion of net gain, that the proposed method achieves tangible and determinable performance improvement, where not only PAPR reduction was considered, but also the reduction in SNR due to applying our technique. As a result, this provides an added advantage for the system designer to tune the operating point of the power amplifier in a manner that achieves maximum system performance, relying on the stable and almost deterministic behavior of the technique.

As for future extensions of this work, we consider further performance and spectral efficiency enhancements by employing compressed sensing in the process of side information transmission [72], [73]. Compressed sensing enables fast encoding of data into a highly compressed set of measurements data. Therefore, we may be able to scale more sub-carriers, and hence further reduce PAPR, without affecting spectral efficiency. This approach is highly appealing especially in the presence of recent fast compressed sensing

decoding mechanisms [74], in addition to its ability to perform efficiently in a highly noisy environment [75], [76].

## APPENDIX

In this appendix, we derive the expected values of the variable $u_i^2$ over the sets $\Omega$ and $\Omega^{\complement}$, as given in (16). From (3), the values of $u_i$ are truncated from above by $\sqrt{\alpha}$. Thus, from (6), this variable will follow a truncated Rayleigh distribution with pdfs given by [69], [77]:

$$f(u_i|i \in \Omega) = \frac{f(u_i)}{1 - F(\sqrt{\alpha})} = \frac{2u_i e^{-u_i^2}}{e^{-\alpha}}$$

$$f(u_i|i \in \Omega^{\complement}) = \frac{f(u_i)}{F(\sqrt{\alpha})} = \frac{2u_i e^{-u_i^2}}{1 - e^{-\alpha}}$$

The above result can be used to evaluate $\mathbb{E}_{i\in\Omega}(u_i^2)$ as follows:

$$\begin{aligned}\mathbb{E}_{i\in\Omega}(u_i^2) &= \int_{\sqrt{\alpha}}^{\infty} u_i^2 f(u_i|i \in \Omega) du_i \\ &= 2e^{\alpha} \int_{\sqrt{\alpha}}^{\infty} u_i^3 e^{-u_i^2} du_i\end{aligned}$$

On the other hand, $\mathbb{E}_{i\in\Omega^{\complement}}(u_i^2)$ can be evaluated as follows:

$$\begin{aligned}\mathbb{E}_{i\in\Omega^{\complement}}(u_i^2) &= \int_0^{\sqrt{\alpha}} u_i^2 f(u_i|i \in \Omega^{\complement})\, du_i \\ &= \frac{2}{1 - e^{-\alpha}} \int_0^{\sqrt{\alpha}} u_i^3\, e^{-u_i^2} du_i\end{aligned}$$

In order to evaluate the above integration, let $s = u_i^2$, and using integration by parts, we get:

$$\int u_i^3\, e^{-u_i^2} du_i = \frac{1}{2} \int s e^{-s} ds = -\frac{1}{2} \left[e^{-s}(s+1)\right]$$

Consequently, we reach:

$$\mathbb{E}_{i\in\Omega}(u_i^2) = 2e^{\alpha} \times -\frac{1}{2}(e^{-\alpha}(1+\alpha)) = 1 + \alpha$$

and

$$\begin{aligned}\mathbb{E}_{i\in\Omega^{\complement}}(u_i^2) &= \frac{2}{1 - e^{-\alpha}} \times \frac{1}{2}(1 - e^{-\alpha}(1+\alpha)) \\ &= \frac{1 - e^{-\alpha}(1+\alpha)}{1 - e^{-\alpha}}\end{aligned}$$

■

## REFERENCES

[1] Y. Huo, X. Dong, and W. Xu, "5G cellular user equipment: From theory to practical hardware design," *IEEE Access*, vol. 5, pp. 13992–14010, 2017.
[2] "IEEE 5G and beyond technology roadmap white paper," IEEE, New York, NY, USA, White Paper, Sep. 2017. [Online]. Available: https://futurenetworks.ieee.org/images/files/pdf/ieee-5g-roadmap-white-paper.pdf
[3] I. F. Akyildiz, S. Nie, S.-C. Lin, and M. Chandrasekaran, "5G roadmap: 10 key enabling technologies," *Comput. Netw.*, vol. 106, pp. 17–48, Sep. 2016.
[4] A. Osseiran, J. F. Monserrat, and P. Marsch, *LTE for 4G Mobile Broadband: Air Interface Technologies and Performance*. Cambridge, U.K.: Cambridge Univ. Press, 2016.
[5] M. R. Palattella *et al.*, "Internet of Things in the 5G era: Enablers, architecture, and business models," *IEEE J. Sel. Areas Commun.*, vol. 34, no. 3, pp. 510–527, Mar. 2016.
[6] M. R. A. Rahim *et al.*, "Service-oriented architecture for IoT home area networking in 5G," in *5G Networks: Fundamental Requirements, Enabling Technologies, and Operations Management*. Hoboken, NJ, USA: Wiley, 2018, ch. 16, pp. 577–602.
[7] E. Dahlman, S. Parkvall, and J. Skold, *4G: LTE/LTE-Advanced for Mobile Broadband*, 2nd ed. Oxford, U.K.: Academic, 2014.
[8] *IEEE Standard for Air Interface for Broadband Wireless Access Systems*, IEEE Standard 802.16-2017 (Revision of IEEE Standard 802.16-2012), Mar. 2018, pp. 1–2726.
[9] J. Kim and I. Lee, "802.11 WLAN: History and new enabling MIMO techniques for next generation standards," *IEEE Commun. Mag.*, vol. 53, no. 3, pp. 134–140, Mar. 2015.
[10] M. S. Afaqui, E. Garcia-Villegas, and E. Lopez-Aguilera, "IEEE 802.11ax: Challenges and requirements for future high efficiency WiFi," *IEEE Wireless Commun.*, vol. 24, no. 3, pp. 130–137, Jun. 2017.
[11] L. Dai, Z. Wang, and Z. Yang, "Next-generation digital television terrestrial broadcasting systems: Key technologies and research trends," *IEEE Commun. Mag.*, vol. 50, no. 6, pp. 150–158, Jun. 2012.
[12] I. Eizmendi *et al.*, "DVB-T2: The second generation of terrestrial digital video broadcasting system," *IEEE Trans. Broadcast.*, vol. 60, no. 2, pp. 258–271, Jun. 2014.
[13] A. M. Rateb, S. K. Syed-Yusof, and N. Fisal, "Improvement of ultra-wideband link performance over bands requiring interference mitigation in Korea," *ETRI J.*, vol. 32, no. 1, pp. 44–52, 2010.
[14] A. M. Rateb, S. K. S. Yusof, and N. Fisal, "Adaptive data distribution technique for enhancing MB-OFDM UWB link performance in detect and avoid environments," *Int. J. Ultra Wideband Commun. Syst.*, vol. 2, no. 1, pp. 1–13, 2011.
[15] C. Sanchis, M.-T. Martínez-Ingles, J.-M. Molina-García-Pardo, J. Pascual-García, and J.-V. Rodríguez, "Experimental study of MIMO-OFDM transmissions at 94 GHz in indoor environments," *IEEE Access*, vol. 5, pp. 7488–7494, 2017.
[16] B. M. Lee, "Improved energy efficiency of massive MIMO-OFDM in battery-limited IoT networks," *IEEE Access*, vol. 6, pp. 38147–38160, 2018.
[17] B. Farhang-Boroujeny and H. Moradi, "OFDM inspired waveforms for 5G," *IEEE Commun. Surveys Tuts.*, vol. 18, no. 4, pp. 2474–2492, 4th Quart., 2016.
[18] S. Venkatesan and R. A. Valenzuela, "OFDM for 5G: Cyclic prefix versus zero postfix, and filtering versus windowing," in *Proc. IEEE Int. Conf. Commun. (ICC)*, May 2016, pp. 1–5.
[19] P. Guan *et al.*, "5G field trials: OFDM-based waveforms and mixed numerologies," *IEEE J. Sel. Areas Commun.*, vol. 35, no. 6, pp. 1234–1243, Jun. 2017.
[20] H. Lin, "Flexible configured OFDM for 5G air interface," *IEEE Access*, vol. 3, pp. 1861–1870, 2015.
[21] D. Wu *et al.*, "A field trial of F-OFDM toward 5G," in *Proc. IEEE Globecom Workshops (GC Wkshps)*, Washington, DC, USA, Dec. 2016, pp. 1–6.
[22] L. Zhang, A. Ijaz, P. Xiao, M. M. Molu, and R. Tafazolli, "Filtered OFDM systems, algorithms, and performance analysis for 5G and beyond," *IEEE Trans. Commun.*, vol. 66, no. 3, pp. 1205–1218, Mar. 2018.
[23] V. Tarokh and H. Jafarkhani, "On the computation and reduction of the peak-to-average power ratio in multicarrier communications," *IEEE Trans. Commun.*, vol. 48, no. 1, pp. 37–44, Jan. 2000.
[24] Y. G. Li and G. L. Stuber, *Orthogonal Frequency Division Multiplexing for Wireless Communications*. New York, NY, USA: Springer, 2006.
[25] M. Senst and G. Ascheid, "Optimal output back-off in OFDM systems with nonlinear power amplifiers," in *Proc. IEEE Int. Conf. Commun.*, Jun. 2009, pp. 1–6.
[26] Y. Rahmatallah and S. Mohan, "Peak-to-average power ratio reduction in OFDM systems: A survey and taxonomy," *IEEE Commun. Surveys Tuts.*, vol. 15, no. 4, pp. 1567–1592, 4th Quart., 2013.
[27] T. S. Rappaport *et al.*, "Millimeter wave mobile communications for 5G cellular: It will work!" *IEEE Access*, vol. 1, pp. 335–349, May 2013.
[28] W. A. Hassan, H. S. Jo, and A. R. Tharek, "The feasibility of coexistence between 5G and existing services in the IMT-2020 candidate bands in Malaysia," *IEEE Access*, vol. 5, pp. 14867–14888, 2017.
[29] W. Hong, K.-H. Baek, and S. Ko, "Millimeter-wave 5G antennas for smartphones: Overview and experimental demonstration," *IEEE Trans. Antennas Propag.*, vol. 65, no. 12, pp. 6250–6261, Dec. 2017.
[30] A.-V. Pham, D. P. Nguyen, and M. Darwish, "High efficiency power amplifiers for 5G wireless communications," in *Proc. 10th Global Symp. Millim.-Waves*, May 2017, pp. 83–84.

[31] R. Gomes, J. Reis, Z. Al-Daher, A. Hammoudeh, and R. F. S. Caldeirinha, "5G: Performance and evaluation of FS-FBMC against OFDM for high data rate applications at 60 GHz," *IET Signal Process.*, vol. 12, no. 5, pp. 620–628, 2018.

[32] T. Jiang and Y. Wu, "An overview: Peak-to-average power ratio reduction techniques for OFDM signals," *IEEE Trans. Broadcast.*, vol. 54, no. 2, pp. 257–268, Jun. 2008.

[33] F. Sandoval, G. Poitau, and F. Gagnon, "Hybrid peak-to-average power ratio reduction techniques: Review and performance comparison," *IEEE Access*, vol. 5, pp. 27145–27161, 2017.

[34] T. A. Wilkinson and A. E. Jones, "Minimisation of the peak to mean envelope power ratio of multicarrier transmission schemes by block coding," in *Proc. IEEE 45th Veh. Technol. Conf. Countdown Wireless 21st Century*, vol. 2, Jul. 1995, pp. 825–829.

[35] T. Jiang and G. Zhu, "OFDM peak-to-average power ratio, reduction by complement block coding scheme and its modified version," in *Proc. IEEE 60th Veh. Technol. Conf. (VTC-Fall)*, vol. 1, Sep. 2004, pp. 448–451.

[36] T. Jiang and G. Zhu, "Complement block coding for reduction in peak-to-average power ratio of OFDM signals," *IEEE Commun. Mag.*, vol. 43, no. 9, pp. S17–S22, Sep. 2005.

[37] T. Jiang, G. Zhu, and J. Zheng, "Block coding scheme for reducing PAPR in OFDM systems with large number of subcarriers," *J. Electron.*, vol. 21, no. 6, pp. 482–489, Nov. 2004.

[38] R. W. Bäuml, R. F. H. Fischer, and J. B. Huber, "Reducing the peak-to-average power ratio of multicarrier modulation by selected mapping," *Electron. Lett.*, vol. 32, no. 22, pp. 2056–2057, Oct. 1996.

[39] S. H. Han and J. H. Lee, "An overview of peak-to-average power ratio reduction techniques for multicarrier transmission," *IEEE Wireless Commun.*, vol. 12, no. 2, pp. 56–65, Apr. 2005.

[40] N. V. Irukulapati, V. K. Chakka, and A. Jain, "SLM based PAPR reduction of OFDM signal using new phase sequence," *Electron. Lett.*, vol. 45, no. 24, pp. 1231–1232, Nov. 2009.

[41] I. Baig and V. Jeoti, "DCT precoded SLM technique for PAPR reduction in OFDM systems," in *Proc. Int. Conf. Intell. Adv. Syst.*, Jun. 2010, pp. 1–6.

[42] D.-W. Lim, J.-S. No, C.-W. Lim, and H. Chung, "A new SLM OFDM scheme with low complexity for PAPR reduction," *IEEE Signal Process. Lett.*, vol. 12, no. 2, pp. 93–96, Feb. 2005.

[43] A. Ghassemi and T. A. Gulliver, "Partial selective mapping OFDM with low complexity IFFTs," *IEEE Commun. Lett.*, vol. 12, no. 1, pp. 4–6, Jan. 2008.

[44] H. B. Jeon, J. S. No, and D. J. Shin, "A low-complexity SLM scheme using additive mapping sequences for PAPR reduction of OFDM signals," *IEEE Trans. Broadcast.*, vol. 57, no. 4, pp. 866–875, Dec. 2011.

[45] M. Breiling, S. H. Miiller-Weinfurtner, and J. B. Huber, "Distortionless reduction of peak power without explicit side information," in *Proc. IEEE Global Telecommun. Conf. (GLOBECOM)*, vol. 3, Nov./Dec. 2000, pp. 1494–1498.

[46] A. D. S. Jayalath and C. Tellambura, "SLM and PTS peak-power reduction of OFDM signals without side information," *IEEE Trans. Wireless Commun.*, vol. 4, no. 5, pp. 2006–2013, Sep. 2005.

[47] S. Y. L. Goff, S. S. Al-Samahi, B. K. Khoo, C. C. Tsimenidis, and B. S. Sharif, "Selected mapping without side information for PAPR reduction in OFDM," *IEEE Trans. Wireless Commun.*, vol. 8, no. 7, pp. 3320–3325, Jul. 2009.

[48] S. H. Müller and J. B. Huber, "OFDM with reduced peak-to-average power ratio by optimum combination of partial transmit sequences," *Electron. Lett.*, vol. 33, no. 5, pp. 368–369, Feb. 1997.

[49] M. Gouda and M. Hussien, "Partial transmit sequence PAPR reduction method for LTE OFDM systems," in *Proc. 4th Int. Conf. Intell. Syst., Modelling Simulation*, Jan. 2013, pp. 507–512.

[50] H.-G. Ryu, J.-E. Lee, and J.-S. Park, "Dummy sequence insertion (DSI) for PAPR reduction in the OFDM communication system," *IEEE Trans. Consum. Electron.*, vol. 50, no. 1, pp. 89–94, Feb. 2004.

[51] C. Siegl and R. F. H. Fischer, "Tone reservation for peak-to-average power ratio reduction in OFDM under different optimization constraints," in *Proc. 13th Int. OFDM Workshop*, 2008, pp. 1–4.

[52] M. Mroue, A. N. J. Palicot, B. Gavalda, and N. Dagorne, "Performance and implementation evaluation of TR PAPR reduction methods for DVB-T2," *Int. J. Digit. Multimedia Broadcast.*, vol. 2010, Aug. 2010, Art. no. 797393.

[53] S. Zabre, J. Palicot, Y. Louet, and C. Lereau, "SOCP approach for OFDM peak-to-average power ratio reduction in the signal adding context," in *Proc. IEEE Int. Symp. Signal Process. Inf. Technol.*, Aug. 2006, pp. 834–839.

[54] Y. Wang, S. Xie, and Z. Xie, "FISTA-based PAPR reduction method for tone reservation's OFDM system," *IEEE Wireless Commun. Lett.*, vol. 7, no. 3, pp. 300–303, Jun. 2018.

[55] R. O'Neill and L. B. Lopes, "Envelope variations and spectral splatter in clipped multicarrier signals," in *Proc. 6th Int. Symp. Pers., Indoor Mobile Radio Commun.*, vol. 1, Sep. 1995, pp. 71–75.

[56] R. van Nee and A. de Wild, "Reducing the peak-to-average power ratio of OFDM," in *Proc. 48th IEEE Veh. Technol. Conf. Pathway Global Wireless Revolution (VTC)*, vol. 3, May 1998, pp. 2072–2076.

[57] H. Chen and A. M. Haimovich, "Iterative estimation and cancellation of clipping noise for OFDM signals," *IEEE Commun. Lett.*, vol. 7, no. 7, pp. 305–307, Jul. 2003.

[58] J. Armstrong, "Peak-to-average power reduction for OFDM by repeated clipping and frequency domain filtering," *Electron. Lett.*, vol. 38, no. 5, pp. 246–247, Feb. 2002.

[59] Y.-C. Wang and Z.-Q. Luo, "Optimized iterative clipping and filtering for PAPR reduction of OFDM signals," *IEEE Trans. Commun.*, vol. 59, no. 1, pp. 33–37, Jan. 2011.

[60] X. Zhu, W. Pan, H. Li, and Y. Tang, "Simplified approach to optimized iterative clipping and filtering for PAPR reduction of OFDM signals," *IEEE Trans. Commun.*, vol. 61, no. 5, pp. 1891–1901, May 2013.

[61] V. Nandalal and S. Sophia, "PAPR reduction of OFDM signal via custom conic optimized iterative adaptive clipping and filtering," *Wireless Pers. Commun.*, vol. 78, no. 2, pp. 867–880, Sep. 2014.

[62] K. Anoh, C. Tanriover, and B. Adebisi, "On the optimization of iterative clipping and filtering for PAPR reduction in OFDM systems," *IEEE Access*, vol. 5, pp. 12004–12013, 2017.

[63] X. Wang, T. T. Tjhung, and C. S. Ng, "Reduction of peak-to-average power ratio of OFDM system using a companding technique," *IEEE Trans. Broadcast.*, vol. 45, no. 3, pp. 303–307, Sep. 1999.

[64] T. Jiang and G. Zhu, "Nonlinear companding transform for reducing peak-to-average power ratio of OFDM signals," *IEEE Trans. Broadcast.*, vol. 50, no. 3, pp. 342–346, Sep. 2004.

[65] T. Jiang, Y. Yang, and Y.-H. Song, "Exponential companding technique for PAPR reduction in OFDM systems," *IEEE Trans. Broadcast.*, vol. 51, no. 2, pp. 244–248, Jun. 2005.

[66] K. Bandara, A. Sewaiwar, and Y.-H. Chung, "Efficient nonlinear companding scheme for substantial reduction in peak-to-average power ratio of OFDM," *J. Syst. Eng. Electron.*, vol. 26, no. 5, pp. 924–931, Oct. 2015.

[67] Y. Rahmatallah, N. Bouaynaya, and S. Mohan, "On the performance of linear and nonlinear companding transforms in OFDM systems," in *Proc. Wireless Telecommun. Symp.*, Apr. 2011, pp. 1–5.

[68] S. P. DelMarco, "A constrained optimization approach to compander design for OFDM PAPR reduction," *IEEE Trans. Broadcast.*, vol. 64, no. 2, pp. 307–318, Jun. 2018.

[69] N. Johnson, S. Kotz, and N. Balakrishnan, *Continuous Univariate Distributions*, 2nd ed. New York, NY, USA: Wiley, 1994.

[70] A. Goldsmith, *Wireless Communications*. Cambridge, U.K.: Cambridge Univ. Press, 2005.

[71] J. Heiskala, J. Terry, and D. Ph, *OFDM Wireless LANs: A Theoretical and Practical Guide*. Indianapolis, IN, USA: Sams Publishing, 2001.

[72] D. L. Donoho, "Compressed sensing," *IEEE Trans. Inf. Theory*, vol. 52, no. 4, pp. 1289–1306, Apr. 2006.

[73] M. Rani, S. Dhok, and R. Deshmukh, "A systematic review of compressive sensing: Concepts, implementations and applications," *IEEE Access*, vol. 6, pp. 4875–4894, 2018.

[74] A. M. Rateb, S.-K. Syed-Yusof, and R. A. Rashid, "A generic top-level mechanism for accelerating signal recovery in compressed sensing," *Digit. Signal Process.*, vol. 69, pp. 237–251, Oct. 2017.

[75] A. M. Rateb and S. K. S. Yusof, "Recovery error bounds on compressed sensing of noisy signals," *Int. J. Commun. Syst.*, vol. 28, no. 3, pp. 546–559, 2015.

[76] A. M. Rateb, S.-K. Syed-Yusof, and R. A. Rashid, "On the impact of prefiltering on compressed sensing in presence of invalid measurements," *IEEE Signal Process. Lett.*, vol. 24, no. 12, pp. 1886–1890, Dec. 2017.

[77] J. F. Lawless, "Truncated distributions," in *Wiley StatsRef: Statistics Reference Online*, N. Balakrishnan, T. Colton, B. Everitt, W. Piegorsch, F. Ruggeri, and J. L. Teugels, Eds. Atlanta, GA, USA: American Cancer Society, 2014.

**AHMAD M. RATEB** received the B.Sc. degree from Ain Shams University, Cairo, Egypt, in 2007, and the M.Sc. and Ph.D. degrees from Universiti Teknologi Malaysia, Johor, Malaysia, in 2009 and 2013, respectively. Since 2013, he has been holding several teaching and research positions in Egypt and Malaysia. He is currently a Lecturer with the Faculty of Electronic and Information Engineering, Huaiyin Institute of Technology, Huai'an, Jiangsu, China. His research interests include compressed sensing, mathematical signal processing, optimization, wireless communications, and 5G technologies.

**MOHAMED LABANA** received the B.Sc. degree from the British University in Egypt, in 2016. He is currently pursuing the M.A.Sc. degree with the Department of Electrical and Computer Engineering, Gina Cody School of Engineering and Computer Science, Concordia University, Montreal, QC, Canada. His research interests include wireless communications and signal processing.